

Integrated two-dimensional simulations of dynamic hohlraum driven inertial fusion capsule implosions

S. A. Slutz, K. J. Peterson, R. A. Vesey, R. W. Lemke, J. E. Bailey, W. Varnum, C. L. Ruiz, G. W. Cooper, G. A. Chandler, G. A. Rochau, and T. A. Mehlhorn
Sandia National Laboratories, Albuquerque, New Mexico 87185-1186

(Received 3 July 2006; accepted 21 August 2006; published online 6 October 2006)

Simulations have been useful for improving the design of dynamic hohlraums for the purpose of imploding inertial fusion capsules [S. A. Slutz, J. E. Bailey, G. A. Chandler *et al.*, *Phys. Plasmas* **10**, 1875 (2003)]. These design changes, which have resulted in capsule implosions with hot dense cores [J. E. Bailey, G. A. Chandler, S. A. Slutz *et al.*, *Phys. Rev. Lett.* **92**, 085002 (2004)] and the production of thermonuclear neutrons [C. L. Ruiz, G. Cooper, S. A. Slutz *et al.*, *Phys. Rev. Lett.* **93**, 015001 (2005)], were based primarily on a series of one-dimensional numerical simulations, which treated the dynamic hohlraum and the capsule implosion separately. In this paper we present simulations which are fully integrated to include the implosion of wire arrays onto foam convertors, the implosion of the capsule imbedded in the foam, and the absorption of radiation into the electrodes. These simulations yield predictions that are in remarkably good agreement with measured values considering the complexity of the problem, which spans more than 100 ns of wire implosion with the subsequent capsule implosion on a few ns timescale. For example, the predicted neutron yields are less than a factor of 2 higher than the measured values, while the predicted shock velocity is about 30% higher than the measured value. The spectroscopically inferred imploded capsule gas core temperatures are somewhat lower than predicted by the simulations, while the gas densities are about a factor of 2 higher. Simulations indicate that a more slowly rising radiation drive temperature yields higher core densities and lower temperatures and thus better agreement with experimental measurements. Possible reasons for a more slowly rising radiation drive are discussed.
 © 2006 American Institute of Physics. [DOI: [10.1063/1.2354587](https://doi.org/10.1063/1.2354587)]

I. INTRODUCTION

Pulsed power is a robust, inexpensive technology, which can deliver large energies efficiently to Z-pinch loads, e.g., the Z accelerator has generated up to 2 MJ of x rays,¹ with efficiencies greater than 15% and an x-ray power exceeding 200 TW. The dynamic hohlraum is an efficient approach to delivering thermal radiation from a Z pinch to an inertial fusion capsule. This concept was developed separately in both the USSR² and the US^{3,4} in the late 1970s, but languished until large number wire arrays were developed as a Z-pinch source.⁵ Through the use of wire arrays, the dynamic hohlraum was developed^{6,7} into an intense radiation source enabling laboratory studies of radiation transport at high radiation temperatures (>200 eV).

Dynamic hohlraums generate intense radiation by driving Z-pinch plasmas into a “convertor,” which is typically made of a low density material such as CH₂ foam. A capsule can be located within the convertor as depicted schematically in Fig 1. A pair of nested wire arrays is typically used to help mitigate the Magneto-Rayleigh-Taylor (MRT) instability.⁸ When the Z-pinch plasma strikes the convertor a shock wave is formed, which propagates inward through the convertor toward the capsule. This shock wave heats the convertor material, which then emits radiation. The convertor is composed of a low opacity material, such as CH₂ foam, so that radiation can easily flow inward to heat an ICF capsule. The wire arrays are composed of a material with high opacity, e.g., tungsten, to minimize the outward flow of radiation. The

material from the wire arrays forms a portion of the case, which surrounds the hohlraum and thermalizes the radiation. The electrodes which form the rest of the case are coated with gold to effectively contain the radiation within the hohlraum.

The development of the dynamic hohlraum configuration on the Z machine has benefited substantially from numerical simulations.^{9,10} A series of one-dimensional (1D) simulations was used to determine optimum values of the radius of the convertor, the density of the foam, the initial capsule radius and the capsule wall thickness. The dynamic hohlraum was first simulated, without a capsule, but with a loss term in the center of the simulation to account for the radiation that would have been absorbed by a capsule if it had been present. The radiation temperature profile history from this simulation was then used in a separate planar simulation of the gold electrode to determine the albedo of the electrodes as a function of time. This time dependent albedo was then incorporated in a subsequent simulation of the dynamic hohlraum. This procedure could be repeated to obtain a self-consistent solution, but generally a single iteration was found to be enough. The final radiation temperature profile was then used to drive a series of 1D spherical capsule implosions to find the optimum capsule parameters for each dynamic hohlraum configuration. Ultimately it was found that a convertor with a density of 14 mg/cm³ and a radius of 3 mm gave near optimum yields for capsules with about a 2 mm diameter. This configuration is now routinely used to im-

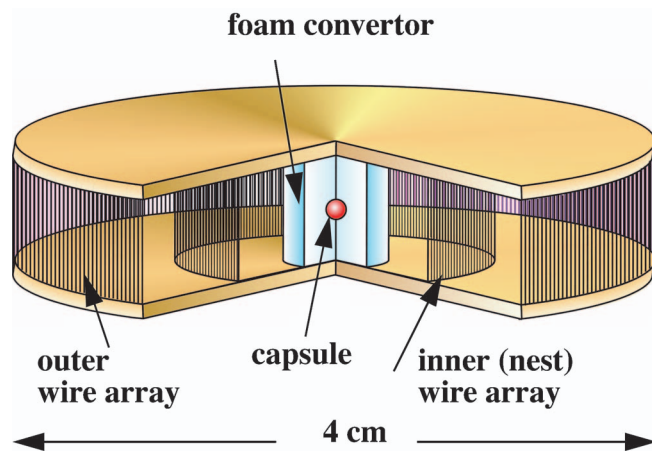


FIG. 1. (Color) A 3D schematic of the dynamic hohlraum configuration.

plode ICF capsules¹¹ with yields of about 10^{11} neutrons per shot. In addition to finding an initial design point, these simulations have helped to improve our understanding of how the dynamic hohlraum operates. As an example, it was recognized prior to these simulations that the collision of the wire-array plasma with the convertor generated a radiative shock, which produced the radiation within the dynamic hohlraum.¹² However, it was assumed that this shock was driven by the material pressure of the wire-array plasma, while the simulations indicate that the momentum of the wire-array plasma is delivered to the shock via the magnetic field pressure.

Even before the achievement of thermonuclear neutron yields with the dynamic hohlraum, numerical simulations¹³ indicated that dynamic hohlraum could be an efficient means of driving high yield inertial confinement fusion (ICF) capsules. These simulations indicated that capsule yields of about 500 MJ could be obtained with approximately 12 MJ of energy delivered to the Z pinch. However, these simulations used the diffusion approximation to radiation transport and thus did not adequately model the effects of radiation asymmetry on the capsule.

Inertial fusion capsules require a high degree of radiation symmetry¹⁴ ($\sim 1\%$ flux variation). An important source of radiation asymmetry within the dynamic hohlraum is caused by the time it takes for the electrodes to heat up. During the initial phase of the implosion the radiation emitted by the electrodes is substantially less intense than the average radiation intensity within the hohlraum. This results in a radiation field at the capsule that is cooler at the poles than at the equator. The re-emission of radiation by the electrodes can be thought of as an effective albedo. This albedo is both time dependent and spatially dependent since different positions on the electrode will experience a different radiation temporal profile. In addition, plasma expands away from the electrode surface as the electrode is heated. This plasma can interact with the incoming wire arrays.¹⁵ Furthermore, the plasma that is ablated from the capsule will eventually interact with the incoming shock wave. Therefore, both the electrodes and the capsule have been integrated into our dynamic hohlraum simulations.

Ultimately we would like to change the design of the dynamic hohlraum so that the radiation driving the capsule is symmetric enough to drive a high yield capsule. Possible design changes include shaping the convertor or providing radiation shields. A design has been presented,¹⁶ which can provide both pulse shaping and adequate radiation symmetry for driving high density capsule implosions. However, further improvements on this design will be needed to obtain high yield capsule implosions. In the process of changing the dynamic hohlraum design to obtain better radiation symmetry on the capsule, one needs a means to measure the radiation symmetry within the hohlraum. This is not a particularly easy task, since there is little diagnostic access. Although one can measure the brightness of thermal radiation along the axis, as is typically done by placing a diagnostic hole at the center of the electrode, one cannot conveniently provide such a hole through the wire-array plasma to directly observe the radiation brightness in the radial direction. A possible solution to this problem is to use a technique that has been developed¹⁷ to determine radiation symmetry by imaging the core of capsule implosions. These imploded cores have been imaged spectroscopically using x rays from dopants such as argon. We have used integrated simulations to design the thin walled capsules that have been used on the Z accelerator to determine radiation symmetry. Comparison of simulated capsule core conditions with spectroscopically determined core conditions is now being used to determine the radiation drive symmetry within the dynamic hohlraum. This ability is critical to the process of designing a dynamic hohlraum with improved radiation symmetry. This process, which involves an interaction between numerical design and experimental testing, as been started and will hopefully advance this concept to a practical driver for inertial fusion.

The agreement between our integrated simulations and various measured quantities is remarkable considering the complexity of the problem and some of the simplifications to the model that were required to make the problem tractable. The simulations include the acceleration of the wire-array plasmas over a period of about 120 ns, the impact of this wire-array plasma with the radiation convertor over a period of about 5 ns, and then the capsule implosion over a period of 2–3 ns. The simulated capsule implosion time from the beginning of the current pulse is within 3 ns of the experimental values. Furthermore, the simulated “clean-2D” (no perturbations in the wire-array plasma or capsule surface to allow the development of instabilities) neutron yields are less than a factor of 2 higher than the measured values. Inclusion of perturbations brings the simulations into even closer agreement. This indicates that a good portion of the appropriate physics is captured by our simulations. However, there are experimentally measured quantities that are significantly different than the simulated values. The predicted shock velocity is about 30% higher than the measured value. The spectroscopically inferred imploded capsule gas core temperatures are about 70% of the mass averaged fuel temperature predicted by the clean-2D simulations, while the measured gas densities are about a factor of 2 higher than predicted. 1D capsule simulations indicate that more slowly rising radiation drive temperatures yield higher core densities

and lower temperatures. We shall show that the inclusion of density perturbations within the wire-array plasma, which allows the simulation to develop instabilities, results in a more slowly rising radiation drive, and simulated capsule core conditions in better agreement with experiments. However, the simulated shock velocity in the convertor remains essentially unchanged. Possible causes for the reduced shock velocity will be discussed.

The integrated approach used to simulate the dynamic hohlraum is described in Sec. II. Insights obtained by these simulations into the basic operation of the dynamic hohlraum are described in Sec. III. The simulation of the capsule implosions and comparison to the experimental results are presented in Sec. IV. The asymmetry of the calculated radiation field and imploded capsule cores are discussed in Sec. V. Conclusions are provided in Sec. VI.

II. 2D INTEGRATED SIMULATION MODEL

The simulations are performed using the 2D radiation magnetohydrodynamics code LASNEX.¹⁸ This code uses an axially symmetric mesh composed of arbitrarily shaped quadrilaterals. The hydrodynamics is Lagrangian, but it is possible to rezone the mesh with an accurate remap of the physical quantities onto a new mesh. We have found that this option is essential to the simulation of the dynamic hohlraum.

The geometry of the dynamic hohlraum experiments presently being tested on Z is shown in Fig. 1. The wire arrays are in the nested configuration that has been used extensively for dynamic hohlraum shots. This configuration has a 240 tungsten wire array (2 mg/cm) at an initial radius of 2 cm and a 120 tungsten wire array (1 mg/cm) at an initial radius of 1 cm. It is believed that the collision of the outer array with the inner array mitigates⁸ the MRT. The initial phase of the wire-array implosion involves the formation of expanding plasmas from each individual wire as it is heated by the current. Due to the limitation of a 2D axially symmetric code, we start our simulations as has been done in previous studies⁶ with two cylindrical tungsten plasmas, each with a thickness of 1 mm, and a temperature of 1 eV, located at the initial positions of the two arrays, see Fig. 2. Due to the large number of wires used in each of the arrays, the expanding plasma from each of the individual wires might be expected to coalesce into two annular plasmas before the plasma is driven inward. However, recent 3D simulations and experimental data^{19,20} indicate that, during the wire initiation process, plasma created from each wire is driven inward as it is ablated before the central core of the wires moves significantly. Although this process was found to be less important as the number of wires is increased, we wanted to estimate the effect of the precursor plasma could have on dynamic hohlraum performance. Since this precursor plasma process cannot be simulated completely by either 1D or 2D codes, we estimated the effect of this process on the radiation drive, by performing simulations with some of the mass of the outer wire array distributed uniformly at zero velocity between the initial position of the outer wire array and the convertor. This resulted in only a small change in the

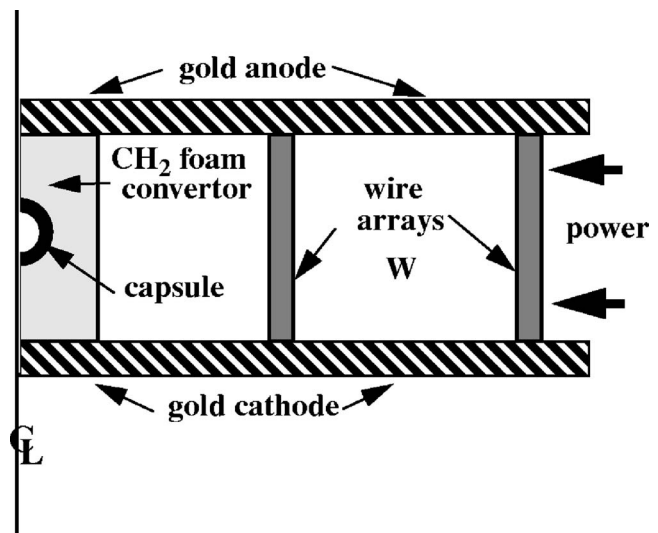


FIG. 2. A 2D schematic of the dynamic hohlraum geometry used for the integrated simulations.

radiation temperature at the capsule location. We also found that the choice of the initial wire array shell thickness and temperature have little effect on the subsequent drive temperature. Therefore, even though we know that the wire-array implosions are more complicated than simple annular plasma implosions, we can expect much of the behavior of the dynamic hohlraum to be modeled reasonably with the annular wire plasma approximation. Of course not all of the behaviors of dynamic hohlraums will be captured by simulations based on this approximation. Such deviations from the results that we report here should be explored when 3D magnetohydrodynamics codes become available.

The electrodes in dynamic hohlraum experiments are coated with gold to minimize the absorption of radiation (wall losses). In our integrated simulations both electrodes were coated with 100 μm of gold extending out to the inner wire array. Separate 1D simulations indicated that the radiation wave would not penetrate all the way through this layer before the capsules were fully imploded. These 1D simulations were also used to determine the appropriate zoning for this region. We found that the zone at the outer surface of the gold layer needed to be quite thin¹⁵ $\Delta z \leq 1 \mu\text{m}$, but the zone size could be increased with depth into the layer without affecting the calculated albedo.

The mesh used in these simulations was designed to be cylindrical outside of the convertor and spherical at the location of the capsule with a transition occurring within the convertor. It was found convenient to regularly remap the mesh back to the original mesh for regions outside of the capsule. Thus that part of the simulation was effectively Eulerian. The location and strength of the shock wave within the convertor as calculated by this Eulerian approach compared well to pure 1D Lagrangian simulations. However, the Eulerian approach required a large number of cells in the capsule to obtain results consistent with 1D Lagrangian simulations of spherical capsule implosions. Therefore an Arbitrary Lagrangian Eulerian (ALE) approach was used in the capsule region.

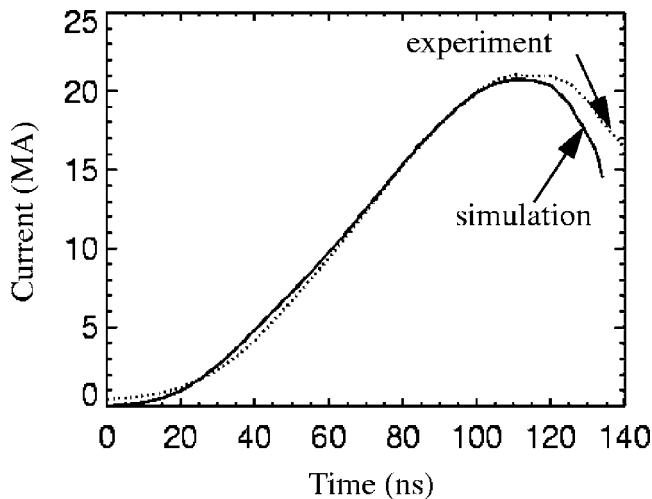


FIG. 3. The drive current is plotted as a function of time both from a typical shot and as computed in a 2D integrated simulation of a dynamic hohlraum implosion.

III. THE OPERATION OF THE DYNAMIC HOHLRAUM

The current driving the dynamic hohlraum simulation is computed using a Thevenin equivalent circuit model of the Z accelerator. The calculated current rises to about 20 MA in 118 ns, in good agreement to the experiments as seen in Fig. 3. The two curves do show some deviation at late times. The lower current in the simulations could be due to an overestimate of the inductance or equivalently an underestimate of the mean radius of the current within the wire-array plasma possibly caused by instabilities. This would imply that the simulations overestimate the pressure driving the wire-array plasma and thus the implosion velocity, shock velocity, and shock strength within the converter. However, it is difficult to know if the difference between these two curves at late time is meaningful since the current monitors can become unreliable after peak current.

The locations of the various materials in a typical simulation are shown in Fig. 4 at different times. The wire arrays have an initial radius of 10 and 20 mm. The foam converter has an initial radius of 3 mm and density of 14 mg/cm^3 . The capsule is a $50 \mu\text{m}$ thick CH shell with a diameter of 2 mm and filled with 24 atm of D_2 . The tungsten plasma is black, the CH_2 converter plasma is green, the D_2 gas is red, and the capsule CH shell is yellow, as is the gold electrode coating. The gold coating and the capsule shell are both initially difficult to see because they are so thin ($<100 \mu\text{m}$), but are more readily visible after they have expanded due to radiative heating. At the time of the second snapshot shown in Fig. 4(b), the two wire-array plasmas are about to collide. Notice that both the inner array and the gold electrodes have expanded considerably due to radiative heat coming from the outer array, which has been resistively heated by the large electrical current ($\sim 20 \text{ MA}$). The final snap shot shown in Fig. 4(c) is when the D_2 gas is near maximum compression. Notice the wire-array plasma has been pushed by the magnetic field into a thin right circular cylinder except for the region near the electrodes where the interaction between the gold electrode plasma and the tungsten wire-array plasma

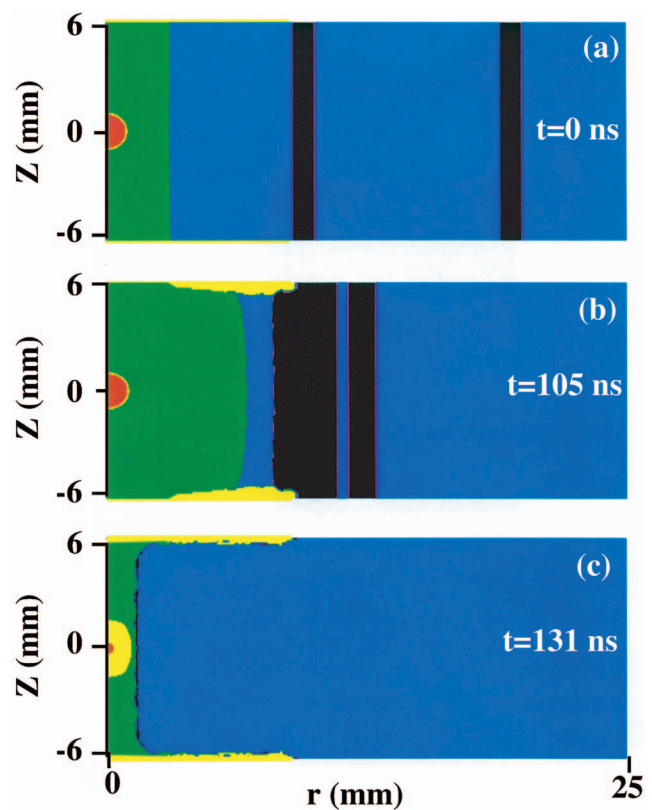


FIG. 4. (Color) Plots of the material locations for three different times in an integrated simulation of a dynamic hohlraum with a capsule imbedded in the foam converter. The tungsten is black, the converter is green, the D_2 is red, and the capsule CH shell and the gold electrode are both yellow.

was important. In this region the gold plasma ablated from the electrode walls has impeded the implosion of the tungsten wire plasma. This actually has a beneficial effect of mitigating the well known wall instability²¹ that normally occurs in Z pinches due to energy absorbed by the electrodes.

The collision of the tungsten wire plasma with the converter generates a strong ($\sim 8 \text{ Mbar}$) high-temperature shock ($500\text{--}800 \text{ eV}$) which propagates into the low density converter. It also drives a shock into the tungsten, but at a lower temperature due to the higher tungsten density and the large magnetic field that is imbedded in the tungsten plasma. The warm tungsten ($\sim 200 \text{ eV}$) radiates nearly as a black body. The strong shock in the foam radiates at a high color temperature ($>500 \text{ eV}$), but is dilute due to the low opacity. This radiation is absorbed by the wire plasma and the gold coated electrodes keeping them at high temperature ($\sim 200 \text{ eV}$). Note that most of the photons within the hohlraum come from re-emission by the tungsten wire plasma.

Contours of the electron temperature are plotted on the top of Fig. 5(a), while the radiation temperature contours are plotted on the bottom for comparison. Profiles of both the radiation and electron temperatures at the midplane are plotted as a function of radius in Fig. 5(b). The electron temperature is significantly higher than the radiation temperature within the shocked region. Note that the ion temperature (not plotted) is only slightly higher than the electron temperature at the shock front and that the electron tempera-

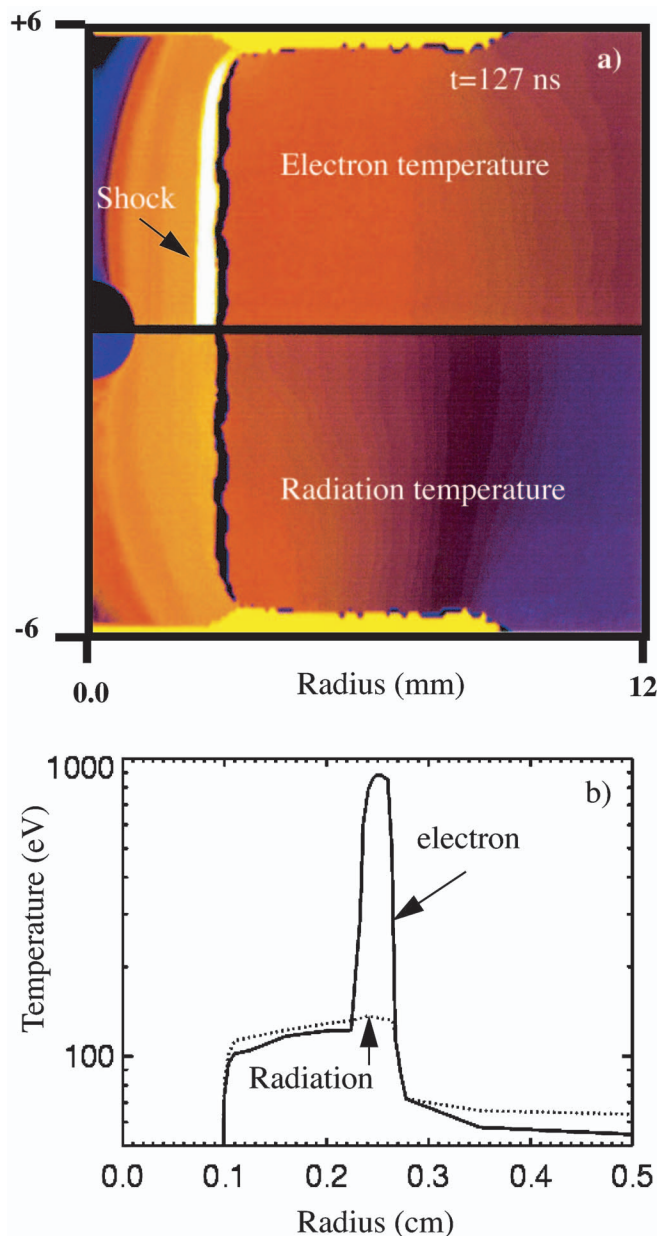


FIG. 5. (Color) Electron and radiation temperatures at the time when the tungsten has reached the original outer radius of the convertor (a) 2D contour plots and (b) 1D plots at the equator as a function of radius.

ture in the shocked region is out of equilibrium with the radiation temperature due to the relatively low opacity of the high temperature CH_2 plasma. The radiation penetrates the foam convertor and reaches the capsule long before the shock does. It can also be seen that the radiation temperature is hotter on the capsule equator than on the poles due to the cooler electrode walls. This asymmetry will be discussed quantitatively later in this paper, see Fig. 21.

The radiation generated by the shock is trapped by the high opacity tungsten plasma. This can be seen by the essentially flat radiation temperature profile within the low opacity foam and the steep drop in the radiation temperature within the high opacity tungsten plasma. Note that the radiation temperature is highest at the shock front position, but only by a few eV. It is because the shock front is optically thin in the

radial direction that the radiation temperature is not larger at the shock front. However, the optical depth in the axial direction is significant, which causes the axially directed radiation intensity to increase at the shock position as has been observed experimentally.¹⁵

We have performed separate simulations with small impurities of high-Z materials added to the CH_2 foam, which indicate that the radiation temperature and the shock temperature can be brought into equilibrium with each other by increasing the opacity of the convertor material. This technique could be useful for maintaining a Planckian spectrum within the hohlraum.

Conditions within the shock wave have been inferred experimentally using spectroscopic techniques.²² The qualitative picture obtained from these measurements is consistent with these simulations; however, the experimentally measured temperature, pressure, and velocity are significantly lower than predicted by the simulations. At the time the simulations predict a shock temperature of 800 eV the measurements indicate a temperature of 400 eV. The shock velocity in the simulations is approximately 4.5×10^7 cm/s while the measurements indicated velocities of approximately 3.3×10^7 cm/s. These discrepancies may be due to 3D effects that are not adequately modeled with a 2D code. We estimate that the Reynolds number in the imploding plasma is fairly large ($>10\,000$), and thus it is possible that the MRT instability leads to turbulence within the wire plasma. Such turbulence would lower the density and increase the ram pressure that the wire plasma could deliver to the convertor material. Note the narrowness of the wire plasma region in Fig. 5(a). In the future we plan to investigate turbulence modeling of the wire plasma to see if this will bring the simulations into better agreement with these shock quantities. We also expect that the inclusion of such effects would lower the calculated drive temperatures. Note that a reduced wire-array plasma density as a result of turbulence would have less effect on the shock velocity in a low density convertor. Indeed simulations and experimental results are in better agreement for lower convertor densities.¹⁵ As we have already mentioned, a current path at larger radius than predicted by the 2D simulations would also reduce the shock velocity and strength.

The radiation brightness temperature exiting the hohlraum through a diagnostic hole (black), the shock position (green), and the capsule radius (red) are plotted as a function of time in Fig. 6. The lines are from the simulations and the symbols are measured values from the experiments. Time equals zero corresponds to the observed peak radial x-ray power in the experiments. All of the simulation results have been time shifted so that the shock positions match up. It should be noted that one can also time tie the simulations to the experiments using the rising portion of the drive current. This results in a time shift of about +3 ns for the simulations. This is a rather small discrepancy considering that the 3D complexities of the wire initiation and precursor plasma generation have not been included in these simulations. On close observation one can see that the shock velocity is smaller in the experiments than for the simulations, and that the capsule

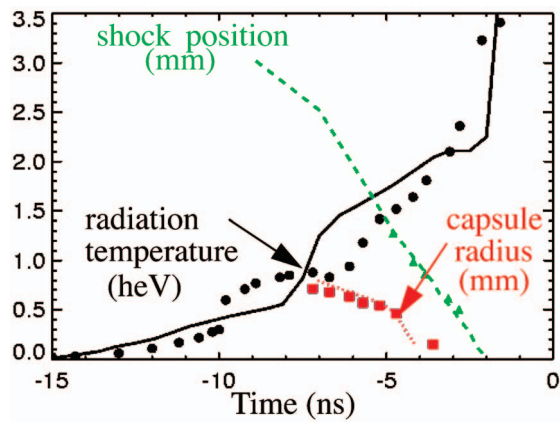


FIG. 6. (Color) Plots of various quantities as a function of time. The curves are the results from the integrated simulations. The symbols are the experimentally measured results. The hohlraum brightness temperature (heV=100 eV) is black, the shock position is green, and the capsule radii are red.

implosion starts later and proceeds more quickly in the simulations. The latter behavior is consistent with the radiation temperature rising more abruptly in the simulations than in the experiments. The radiation brightness temperature within the hohlraum was inferred experimentally by measuring the x-ray intensity exiting a hole in the electrode. The position of the capsule was determined from gated x-ray pinhole images. The radiation brightness exiting the diagnostic hole is not exactly the same as the radiation temperature at the capsule. The curve in Fig. 6 is the calculated brightness temperature exiting the diagnostic hole. These types of measurement have been reported previously for dynamic hohlraums with a larger less dense convertor.²³

IV. CAPSULE IMPLOSIONS: NEUTRON YIELDS AND CORE CONDITIONS

Thin walled capsules have been used in dynamic hohlraum experiments so that the imploded gas cores can be observed spectroscopically. The response of these capsules to the radiation drive generated within these dynamic hohlraum experiments is illustrated by the results of a 1D HYDRA (Ref. 24) capsule simulation using a time-dependent radiation temperature boundary condition consistent with the integrated LASNEX simulations. In this simulation the capsule was composed of a CH shell of inner diameter 2 mm and thickness of 50 μm filled with deuterium at a pressure of 24 atm. The density, electron temperature, and radiation temperature are plotted as a function of radius at several times in Fig. 7. At the earliest time ($t=128.0$ ns), the radiation has just started to penetrate into the CH shell generating a strong shock wave in the CH as seen in Fig. 7(a). Several shock waves are then generated as the radiation temperature rises. These shock waves compress the CH to roughly four times the initial density as seen in Fig. 7(b). At this point the compressed shell expands (explodes) and becomes optically thin to the driving radiation as can be seen in Fig. 7(c). Notice that at this point the shell is still at approximately 80% of the initial radius. Thus except for the initial increase in density, these simulated capsule implosions are similar to “exploding

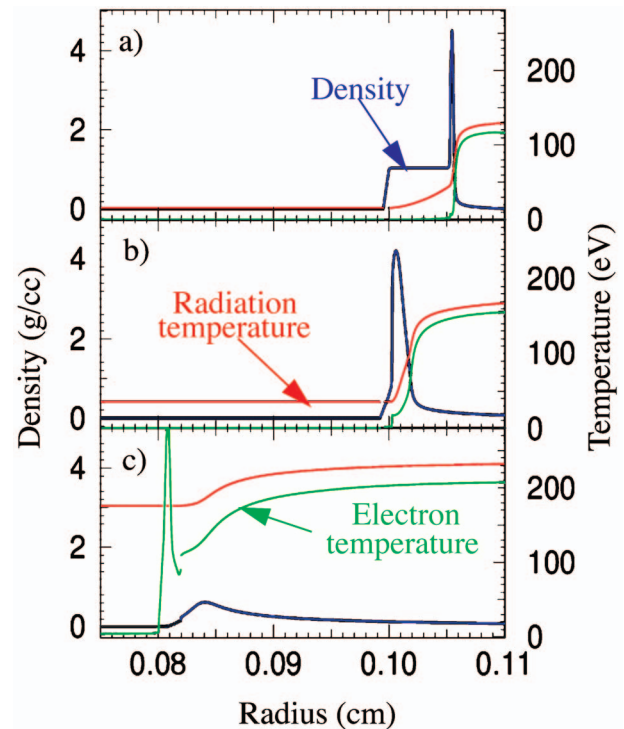


FIG. 7. (Color) The results of a radiation driven capsule simulation as calculated using the HYDRA code are plotted as a function of radius, density (blue), radiation temperature (red), and electron temperature (green). The plots are at three times during the simulation: (a) $t=128.0$, (b) $t=128.9$, (c) $t=130.1$.

pusher” capsules²⁵ that were used in the early inertial fusion experiments driven by lasers. The implosion behavior is further illustrated by Fig. 8, which is a set of time-dependent plots of the peak density in the CH ablator, the mass averaged density in the deuterium fuel, the peak deuterium ion temperature, and the mass averaged fuel ion temperature. The density peaks twice within the CH shell due to subsequent shocks and then falls as the average ablator (CH shell)

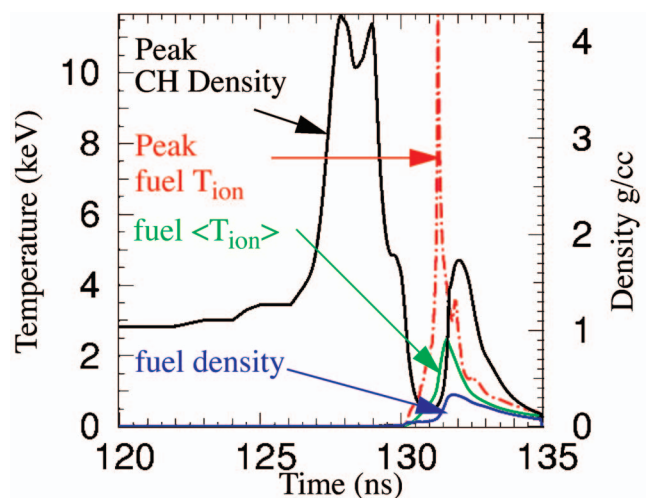


FIG. 8. (Color) Peak CH ablator density, mass averaged deuterium fuel density, peak deuterium ion temperature, and mass averaged deuterium ion temperature, as calculated in a HYDRA simulation, are plotted as a function of time.

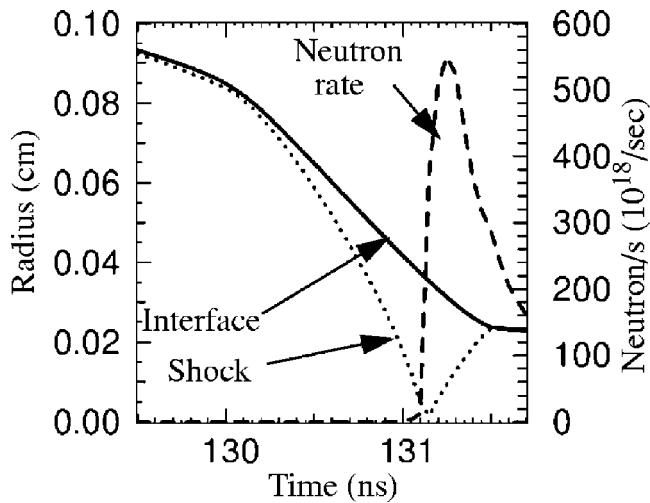


FIG. 9. The deuterium/ablator interface, shock position within the deuterium, and the neutron production rate, as calculated in a HYDRA simulation, are plotted as a function of time.

temperature starts to rise. The explosion of the CH shell then compresses the deuterium, which rises to a peak average density of about 0.3 g/cm^3 . The deuterium temperature peaks slightly before the peak average density. This is because the peak temperature occurs when the first strong shock within the fuel reaches the center. The average density continues to increase as a stagnation shock propagates outward. This stagnation shock can be seen in Fig. 9, which is a time-dependent plot of the shock and the shell/deuterium interface position. The neutron generation rate is also plotted. Notice that the peak neutron generation rate occurs just after the shock hits the center of the fuel and this rate has fallen substantially by the time the ablation shock propagates outward to the CH/deuterium interface (about 400 ps), thus there is very little “compressive yield” as is typical of exploding pusher capsules.

It should be noted that simulations indicate that simply thickening the shell does not lead immediately to a more ablative implosion. This is because increasing the shell thickness causes the capsule to implode later in time, but the radiation temperature within the dynamic hohlraum is rising rapidly (see Figs. 6 and 15) allowing it to penetrate the shell. However, ablative behavior can be produced by simultaneously decreasing the shell diameter and modestly increasing the shell thickness so that the implosion time is maintained constant. Such capsules have not yet been tested, because the simulations indicate that the CH shell would be opaque to the spectroscopic lines emitted by the argon dopant that is presently being used. We expect to test such ablative capsules as neutron diagnostics are improved and the use of dopants emitting more energetic x rays is developed.

The neutron yields as calculated from integrated LASNEX simulations are plotted as a function of capsule wall thickness in Fig. 10 and as a function of capsule diameter in Fig. 11. These capsules consisted of a shell of CH filled with deuterium (D_2) at pressures of about 24 atm. A small amount of argon (0.085 atm) was added to the D_2 for x-ray spectroscopic measurements. Note that capsule implosions with no

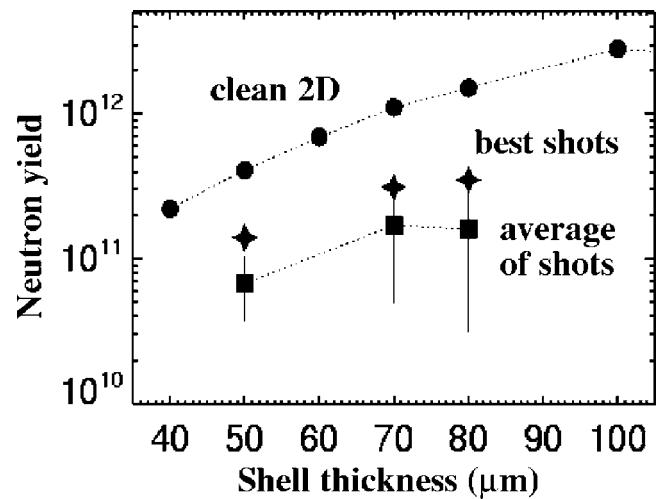


FIG. 10. Neutron yields from 2 mm diameter CH capsules filled with D_2 gas are plotted as a function of capsule shell thickness. The circles are the results obtained from 2D integrated simulations without any perturbations in the wire array, “clean 2D.” The stars are the best experimental results and the squares are the average experimental yields. The error bars are one sigma calculated from the variation in the yields.

argon added to the deuterium had statistically the same yield. The circles are the calculated yields from 2D integrated simulations without any perturbations applied to the wire plasma to seed the MRT instability. The stars are the best experimental yields obtained at each of the shell thicknesses and the squares are the average of the experimental yields obtained at each shell thickness. The vertical lines are error bars based on the shot to shot variation (one standard deviation). The simulations predicted that the capsule yield should increase with the capsule diameter up to a diameter of about 2.5 mm as is clearly observed experimentally. The simulations also predicted that the neutron yield should increase with shell thickness. This trend is realized reasonably well by the best experimental yields, but at a reduced yield. How-

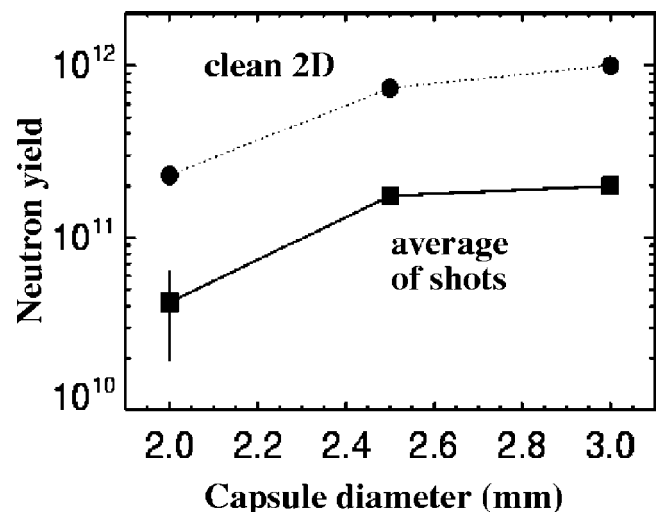


FIG. 11. Neutron yields from CH capsules, with a shell thickness of $70 \mu\text{m}$, filled with D_2 gas are plotted as a function of capsule diameter. The circles are the results of 2D integrated simulations and the squares are the average experimental yields.

ever, this trend is not as apparent in the average yields and was not evident at all when we first obtained neutron signals from capsules. There has been a fairly steady improvement in the neutron yields, which we attribute to improvement in the fabrication of the capsules.²⁶

Despite the fairly good agreement between the simulated neutron yields and the experimental results, there are some measurements that differ significantly from the simulation results. Spectroscopic measurements^{26,27} of the imploded capsule core conditions indicate that the deuterium density is a factor of about 2 times higher than predicted by the simulations and the average temperature within the deuterium is also about 70% of the simulation results. Furthermore, the shock velocity in the convertor has been measured to be approximately $33 \text{ cm}/\mu\text{s}$ as compared to the simulations which predict velocities of $40\text{--}45 \text{ cm}/\mu\text{s}$. We believe that these two differences are related, since a slower shock velocity implies that the radiation temperature should rise more slowly and simulations indicate that a slower rising radiation temperature results in cooler and denser implosions. Possible causes for this discrepancy in the simulation results are 3D effects in the wire implosion initiation, the nonhomogeneous nature of the convertor foam, and the unstable nature of Z-pinch implosions.

In the experiments the convertors are constructed from CH_2 foams with densities of approximately $14 \text{ mg}/\text{cm}^3$. In our simulations this is modeled as a homogeneous mixture of C and H despite the fact that the foam consists of thread-like portions of solid CH_2 with diameters of a few μm separated from each other by about $20 \mu\text{m}$. We were concerned that the heterogeneous nature of the foam could have significant effects on the effective equation of state (EOS) or the effective opacity of the foam. These effects could either change the shock velocity or allow radiation to penetrate to the capsule at an earlier time. We performed two separate 2D simulations using the geometries shown in Fig. 12. In the first simulation, the foam is represented by a periodic array of annular filaments of CH_2 with an outer radius $R_{\text{conv}}=3 \text{ mm}$, and inner radius $R_{\text{cap}}=1 \text{ mm}$, and a thickness of $1 \mu\text{m}$ at normal solid density as shown in Fig. 12(a). In the second simulation the foam is represented by number of randomly located filaments, as shown in Fig. 12(b). The dashed lines are periodic boundary conditions. To avoid unneeded complexity, the capsule is approximated as a hollow pipe with a wall of thickness $50 \mu\text{m}$, which was composed of CH at normal solid density, $1.04 \text{ g}/\text{cm}^3$. A radiation temperature boundary condition is applied to the outer radius of these simulations. This radiation temperature was obtained from the outer boundary of the convertor in a simulation of the dynamic hohlraum using the geometry of Fig. 2. The radiation that first reaches the convertor is due to the joule heating of the wire arrays before they implode. This radiation rises continuously from the beginning of the current pulse up to a value of about 50 eV just prior to the collision of the wire-array plasmas with the convertor at about 115 ns into the simulation. This radiation heats the foam filaments, which then expand and coalesce forming an essentially homogeneous plasma at about $75\text{--}80 \text{ ns}$ into the simulation. This is long before the wire-array plasma collides with the con-

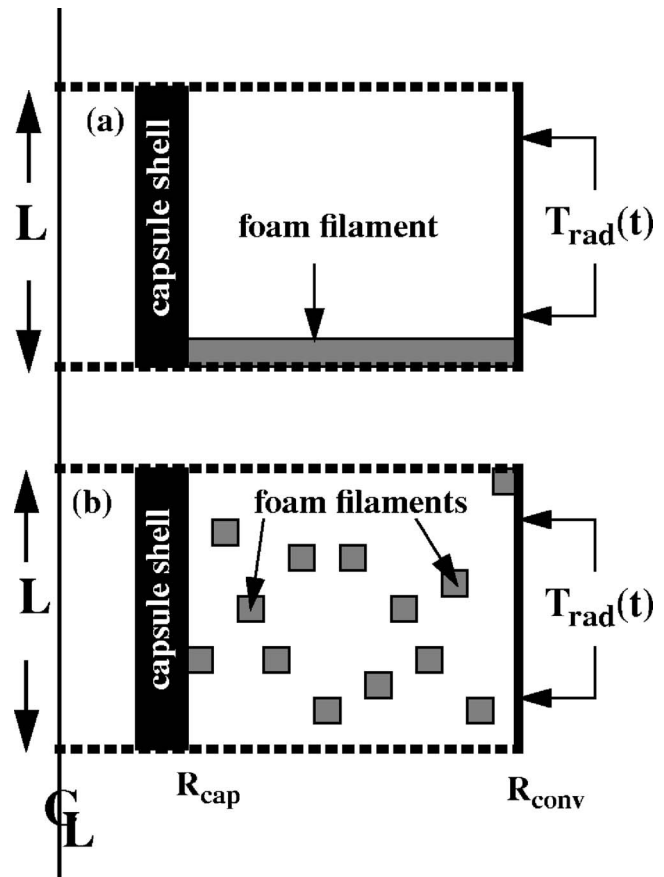


FIG. 12. Geometries for simulating inhomogeneous CH_2 foams. (a) Periodic thin disks; (b) random flakes.

vertor and generates the shock wave, which is the source of the thermal radiation that drives the capsule implosion. Thus it is unlikely that using a homogeneous EOS for the foam will introduce a significant error in calculating either the shock velocity or the radiation drive. In both of these heterogeneous foam simulations the radiation temperature at the capsule peaks at about 1.5 eV just prior to the coalescence of the filaments. In comparison, the temperature at the capsule is essentially zero at this time in a simulation with homogeneous foam because the radiation wave has not yet penetrated the foam. The radiation temperature at the capsule from both homogeneous and heterogeneous foam convertors was then used to drive two 1D spherical capsule implosion simulations. These implosions were essentially identical, which justifies our use of a homogeneous model for our 2D simulations. However, it is possible that the radiation that reaches the capsule before the coalescence of the filaments could introduce small perturbations on the capsule surface that could seed the Rayleigh-Taylor (RT) instability. We do not expect such perturbations would have a dramatic effect on the thin-walled capsules experimented with on the Z, but this issue should be revisited when the experiments develop to using thick walled ablative capsules, which will be more susceptible to the RT instability.

The wire-array implosions are unstable even when they are represented as simple annular plasmas. First, they are Rayleigh-Taylor unstable due to the acceleration of the wire-

array plasma by the essentially zero density magnetic field. They are also unstable because the magnetic pressure is proportional to the inverse square of the radius. The combination of these two effects is referred to as the Magneto-Rayleigh-Taylor (MRT) instability. Despite this instability, simulations of wire-array plasma implosions will not exhibit the characteristic bubble and spike features unless an initial perturbation is applied to the wire-array plasma. A convenient way to impose such a perturbation is to randomly vary the initial density of the wire plasma on a cell to cell basis. In practice a numerical function (random number generator) is used that produces a sequence of numbers with a uniform probability density between $(-1, 1)$. Each number in this sequence is multiplied a fixed fraction of the average density in the region (perturbation level). The result is then added to the average density to determine the initial density of each subsequent cell. The sequence of numbers depends on an initial seed number set in the function. One can vary this “random number seed” to see if the results depend on the details of the cell to cell density variations.

So far we have only considered simulations without perturbations of the wire-array plasmas. This is a reasonable first approximation, since previous simulation work²⁸ indicated that the shock structure, which drives the radiation within the dynamic hohlraum, is quite insensitive to such perturbations. This insensitivity is due to the stability of the shock wave itself and to the snowplow stabilization of the wire-array plasma. The latter effect can be readily seen in Fig. 13, which shows contour plots at two different times during an implosion as calculated with a LASNEX simulation using initial random density perturbations of 0.35% in the outer wire array. Note the magnitude of the Rayleigh-Taylor spikes in the wire-array plasma (black) has decreased significantly at the later time due to the stagnation of this plasma against the convertor material (green). However, despite this partial stabilization, the MRT instability will still reduce the ability of the high- z wire-array plasma to trap radiation within the hohlraum. This can be seen in Fig. 14 which is a plot of the Rosseland optical depth in the radial direction as a function of the axial position, z . As can be seen, the optical depth varies considerably and in some regions is less than unity. These thin regions would look cool to a capsule and introduce asymmetries to the radiation field at the capsule.

We have found that various simulated quantities, such as the neutron yield, depend significantly on the level of perturbations applied to the outer wire array. Perhaps a little more surprising we have found that the results also depend significantly on the random number seed. This is because changing the seed number changes the location of the bubbles and spikes. If a bubble happens to be close to the capsule, the radiation temperature is reduced by the increased radiation losses through the wire-array plasma. This affects both the yield and the symmetry of the implosion. Indeed such a process may be occurring in the actual experiments, which do exhibit significant (factors of 2–3) shot-to-shot variations in the neutron yield.

We ran 10 sets of simulations with perturbation levels in the outer wire-array plasma of 0.0%, 0.25%, 0.5%, 0.75%, and 1.0% for two different capsule shell thicknesses of 50

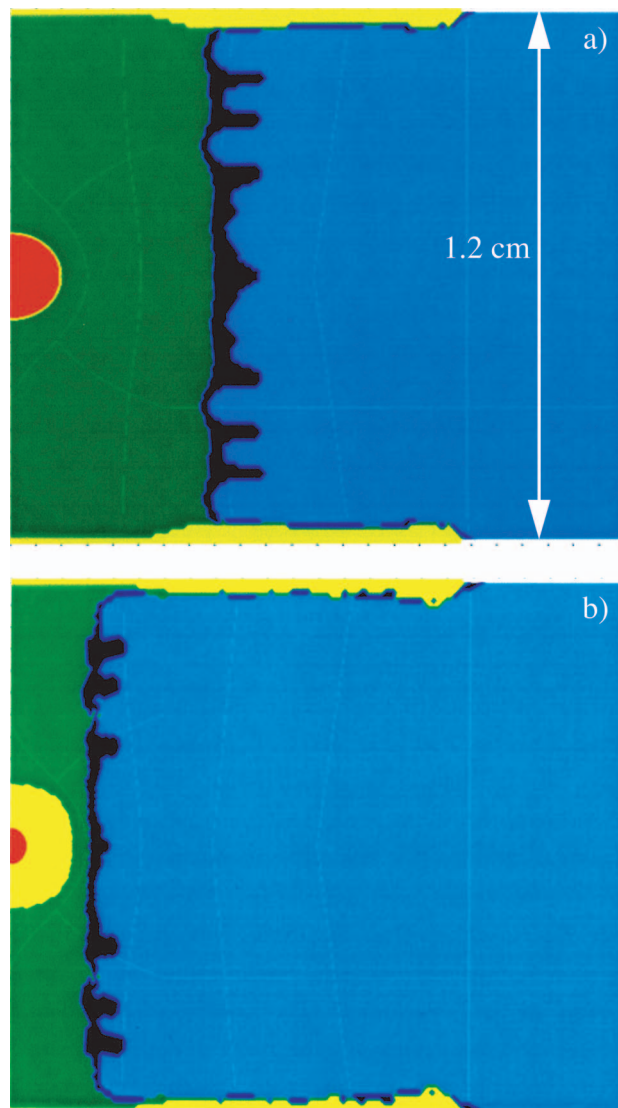


FIG. 13. (Color) Contour plots from an integrated 2D simulation showing the materials at two different times during the implosions, (a) $t=124.9$ ns, and (b) $t=130.6$ ns. The density of the outer wire-array plasma was perturbed cell to cell with amplitudes of 0.35% to seed the Magneto-Rayleigh-Taylor instability.

and $70 \mu\text{m}$. Each of these sets consisted of 9 simulations with different random number seeds (90 simulations in all). The ensemble averaged radiation temperatures are plotted as a function of time in Fig. 15 for simulations with perturbation of 0.0%, 0.5%, and 1.0%. The radiation temperature is somewhat higher at early times for the simulations with larger wire-array perturbations due to the faster arrival of the bubbles generated within the wire-array plasma. The situation is reversed at later times when the trapping of the radiation becomes more important because of the higher radiation temperature. The more slowly rising radiation drive produced by perturbed wire-array plasmas result in a reduction of the neutron yield as can be seen in Fig. 16, which is a plot of the neutron yields from 2 mm diameter, 50 and $70 \mu\text{m}$ thick CH shell capsules as a function of the perturbation strength. A 1 sigma variation as a function of the random seed is shown as vertical bars. Clearly increased wire-array

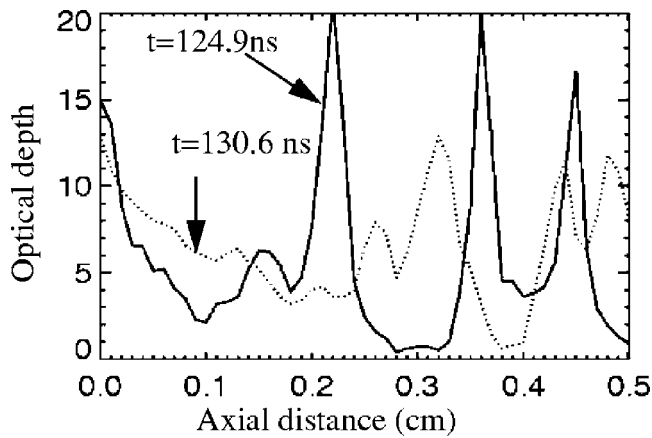


FIG. 14. The Rosseland optical depth through the wire-array plasma is plotted as a function of the axial position, z . These results are for the same simulation shown in the previous figure. The solid curve is for $t = 124.9$ and the dotted curve is for $t = 130.6$.

perturbation brings the simulated yields into better agreement with the experimentally measured yields. It is also interesting that the perturbations of the wire-array plasma have a much larger effect on the thicker walled capsule. This is probably because these capsules implode later and the late time drive is reduced. Furthermore, the symmetry of the thicker walled capsule capsules is more strongly affected by increased strength of the wire-array perturbations. Again this is probably because of the later implosion time, which allows the wire-array plasma to approach the capsule more closely thus reducing the case-to-capsule-ratio and increasing the radiation asymmetry. The fuel densities and temperatures of the compressed cores are also affected by the change in the drive profile. The mass averaged core densities are plotted in Fig. 17. The spectroscopically inferred densities are indicated by the horizontal dashed lines, black for $50 \mu\text{m}$ shell thickness and red for $70 \mu\text{m}$. Clearly increasing the perturbation level brings the simulated results into closer agreement with the spectroscopically determined average fuel density. The mass averaged core electron temperatures are

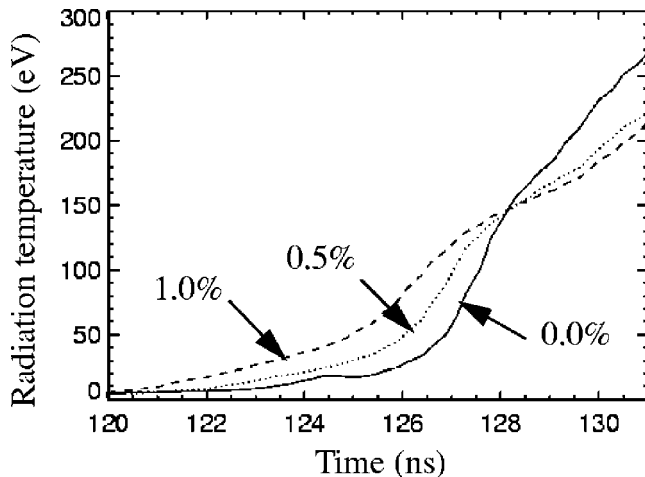


FIG. 15. The ensemble averaged radiation temperatures at the capsule surface from integrated simulations with three different levels of perturbations are plotted as a function of time.

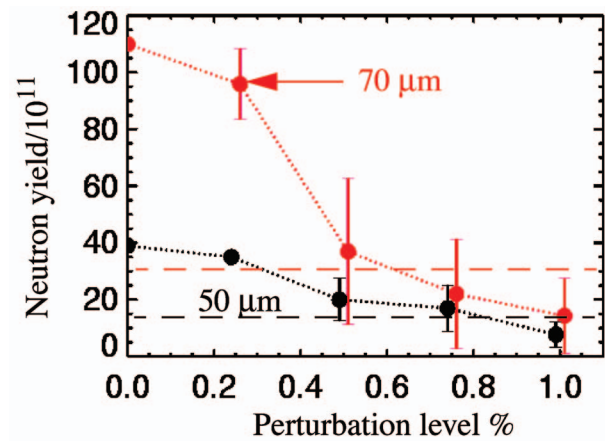


FIG. 16. (Color) The average neutron yields (circles) from a series of simulations with 2 mm diameter capsules are plotted as a function of the perturbation amplitude. The vertical bars indicate the 1 sigma variation of 9 simulated yields with different initial random number seeds. The circles are the average of these yields. The dashed horizontal lines indicate the best experimental yields. Black curves are for $50 \mu\text{m}$ and red curves are for $70 \mu\text{m}$ thick shells.

plotted in Fig. 18. Again the spectroscopically inferred temperatures are indicated by horizontal dashed lines and increased perturbation level brings the simulation results into better agreement with the experimental results. Note that any effect that causes the radiation temperature to rise more slowly would similarly affect the imploded capsule core conditions. The measured fuel temperature is about 70% of the unperturbed (clean 2D) simulation results, while the measured fuel density is about a factor of 2 higher than indicated by the 2D clean simulations. Inspection of Figs. 17 and 18 indicates that a perturbation of about 1.0% is required to bring the simulation and experimental results into agreement. At this perturbation level, the simulations exhibit large

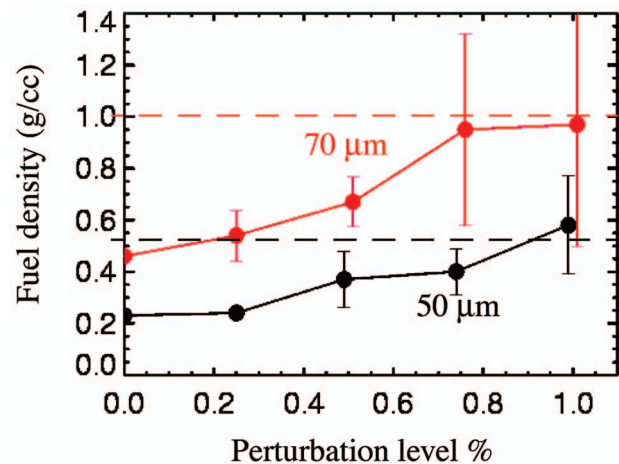


FIG. 17. (Color) The average of the peak mass averaged fuel densities, from the same series of simulations as Fig. 16, is plotted as a function of the perturbation amplitude. The vertical bars indicate the 1 sigma variation of 9 simulated peak mass averaged fuel densities with different initial random number seeds. The circles are the average of these peak mass averaged densities. The dashed horizontal lines indicate the spectroscopically inferred fuel densities. Black curves are for $50 \mu\text{m}$ and red curves are for $70 \mu\text{m}$ thick shells.

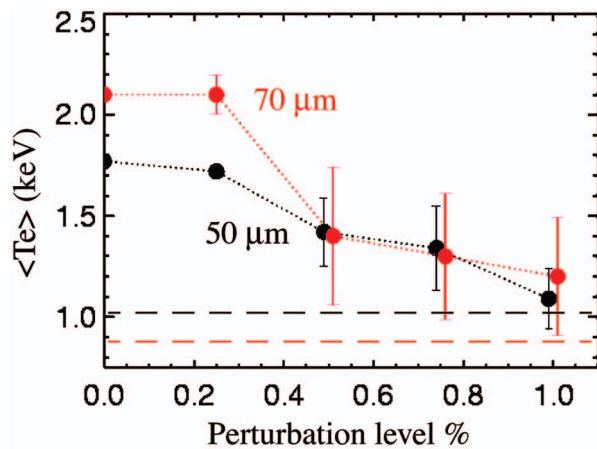


FIG. 18. (Color) The average of the peak mass averaged fuel electron temperatures, from the same series of simulations as Fig. 16, is plotted as a function of the perturbation amplitude. The vertical bars indicate the 1 sigma variation of 9 simulated peak mass averaged fuel electron temperatures with different initial random number seeds. The circles are the average of these peak mass averaged electron temperatures. The dashed horizontal lines indicate the spectroscopically inferred fuel temperatures. Black curves are for 50 μm and red curves are for 70 μm thick shells.

fluctuations of the areal density (optical depth) in the wire-array plasma, which could have a deleterious effect on the radiation symmetry within the hohlraum, since there will be regions of very low optical depth in the wire-array plasma, as indicated in Fig. 14 (which was for a simulation with an amplitude of only 0.35%). Note that the simulations with initial perturbation strengths of 1.0% do indeed show a large variation in the symmetry of the capsule implosions, which are generally highly oblate and often dumbbell in shape. It is interesting to note that a recent thick walled beryllium capsule implosion had a double lobed core indicative of a dumbbell shaped implosion. One should note that the magnitude of the radiation asymmetry produced by the MRT is probably over estimated in 2D simulations due to the existence of only $m=0$ modes, but our results still suggest that the MRT may limit the practicality of the dynamic hohlraum concept. The existence of regions of low optical depth (holes) in the wire-array plasma could be a fatal flaw to this concept, since the asymmetries produced in the radiation field at the capsule would be random and would not be removed by simple design changes such as radiation shields or capsule shimming.

We are planning to make spatially resolved measurements of the optical depth of the wire-array plasma to determine the importance of this effect. If the wire-array plasma has regions of low optical depth, we will have to explore design changes to mitigate this problem such as adding high- z material to the outside of the convertor.¹⁶ This material would contribute to the total optical depth of the wire plasma and could potentially fill in the holes if the MRT is not too virulent.

We emphasize that the formation of optically thin regions in the wire-array plasma due to MRT instabilities may not be the cause of the difference between the simulated capsule core conditions and the measured values. Any phenomenon that decreases the rate of the radiation temperature rise within the hohlraum could have this effect. Recall that

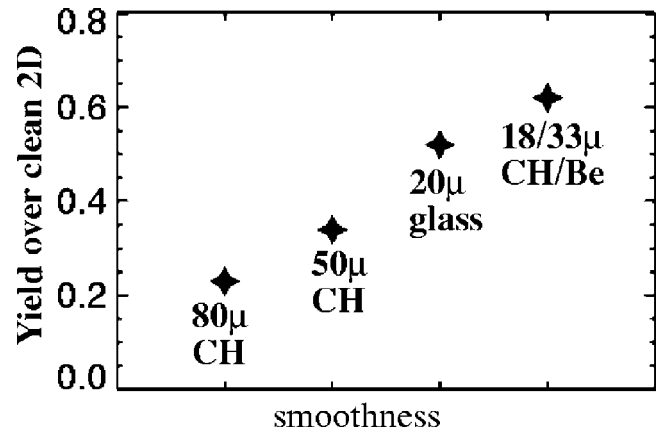


FIG. 19. The ratios of the experimentally measured neutron yields over the unperturbed (clean 2D) integrated simulations are plotted for several capsule shell compositions and thicknesses. The surface roughness of these capsules decreases to the right.

the measured shock velocity is lower than the simulations predict, yet introducing perturbations to the wire-array plasma in a 2D simulation has very little effect on the simulated shock velocity. As we have previously mentioned the shock velocity could be affected by turbulence generated by the MRT instability within the wire-array plasma. This could have the effect of thickening the wire-array plasma without necessarily producing holes. Thicker (lower density) wire-array plasmas would exert less RAM pressure on convertors and thus drive shocks with lower velocities. This would result in a more slowly rising radiation temperature within the dynamic hohlraum. As we have shown, radiation driven capsule simulations indicate that increasing the risetime of the radiation temperature both lowers the peak fuel temperature and increases the fuel density. Since this thickening mechanism does not require regions of low optical depth, the symmetry of the radiation might not be adversely affected. Similarly a late time reduction in the drive current due to a parallel current path could have a similar effect. Clearly it is important to determine what mechanism is responsible for the discrepancy. We plan to incorporate a turbulence model²⁹ into our simulations of the dynamic hohlraum in future studies and options for introducing a parallel current path in the simulations will be explored.

The ratios of the experimentally measured neutron yields over the clean-2D simulated yields (YOC) are plotted in Fig. 19. The surface roughness of the CH capsules was measured to be about 1 μm rms. Capsules which were fabricated from glass or CH coated with beryllium, had much smoother outer surfaces. The glass shelled capsules had a surface roughness of about 0.2 μm , while the beryllium capsules had a surface roughness of approximately 0.1 μm . The trend of Fig. 19 suggests that YOC increases with smoothness of the outer surface.

High resolution 2D simulations of capsule implosions were performed using HYDRA to study the effect of surface roughness on the performance of these capsules. The capsules were driven with a symmetric radiation drive with a time-dependent radiation temperature obtained from the 2D integrated LASNEX simulations with a perturbation level of

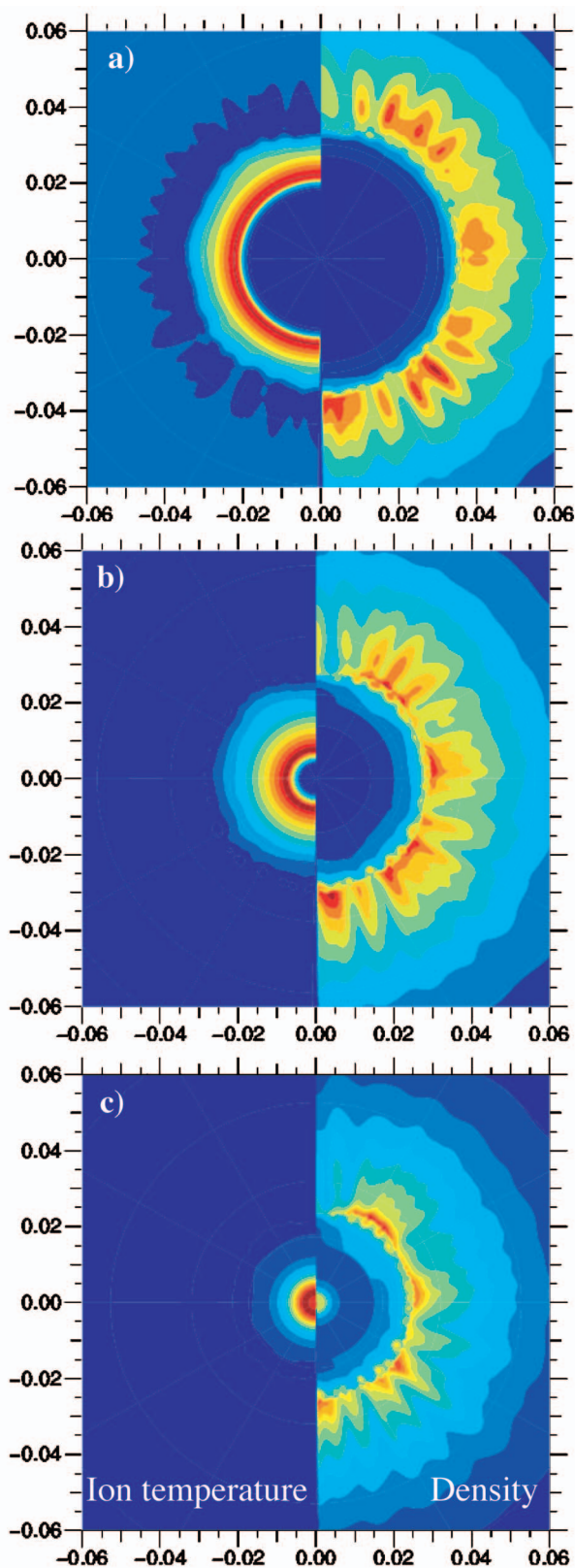


FIG. 20. (Color) Contour plots of the ion temperature (left) and the density (right) from a HYDRA simulation of a $50\ \mu\text{m}$ thick $2.0\ \text{mm}$ diameter CH capsule with a surface roughness of approximately $1\ \mu\text{m}$ RMS at different times during the implosion.

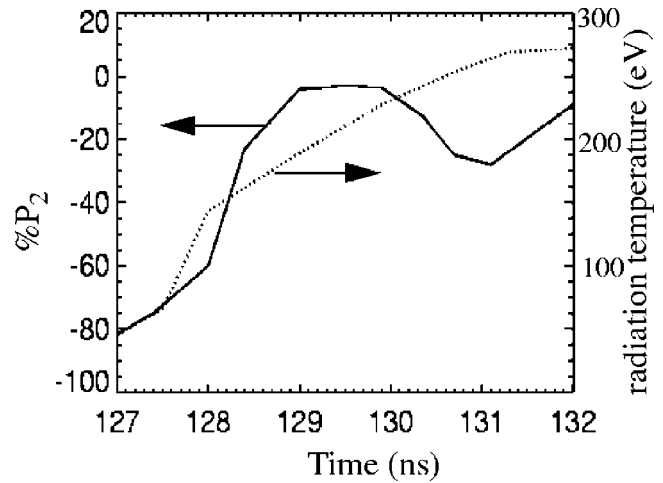


FIG. 21. The amplitude of the second Legendre mode of the radiation flux at a capsule in an integrated simulation is plotted as a function of time. The radiation temperature at the capsule is also plotted for comparison.

1.0%. Figure 20 shows contour plots obtained by such a simulation at several times during the implosion of a CH capsule with a surface roughness of $1\ \mu\text{m}$. The ion temperature is plotted on the left and the density is plotted on the right. As previously discussed, shock waves are generated by the initial ablation of the outside of the shell. Without surface roughness, this shock wave increases the density of the shell material by about a factor of 4, until the shock reaches the inner surface of the shell. Then a rarefaction wave is sent back outward and the shell starts to explode. As the density decreases the shell becomes optically thin to the drive radiation and the implosion continues in an exploding pusher mode. In the case of a perturbed capsule, the shell is broken up azimuthally [Fig. 20(a)] at the time the capsule would normally have reached peak density. The explosion of this broken up shell does not produce as large a radial implosion velocity as the unperturbed case because some of the expansion energy results in azimuthal rather than radial motion. Thus although the ion temperature contour plots show the shock wave remains spherical, the yield is reduced roughly a factor of 2 by the lower shock velocity. This may explain the improved YOC for the smoother glass and beryllium capsules.

V. RADIATION AND CORE SYMMETRY

An important reason for developing an integrated simulation capability is to determine the radiation asymmetries present in the dynamic hohlraum. The second Legendre mode, P_2 , of the radiation asymmetry, as calculated at the capsule surface from an integrated unperturbed simulation, is plotted as a function of time in Fig. 21. The radiation drive temperature is also plotted (dotted line). Initially the radiation field is equator hot, but the drive temperature is not very high at this time. The symmetry improves as the radiation temperature increases, due to the heating of the electrodes. The asymmetry will become pole hot late in time when the shock reaches the axis, but this is after the capsule implodes, which occurs between 130 and 132 ns depending on the cap-

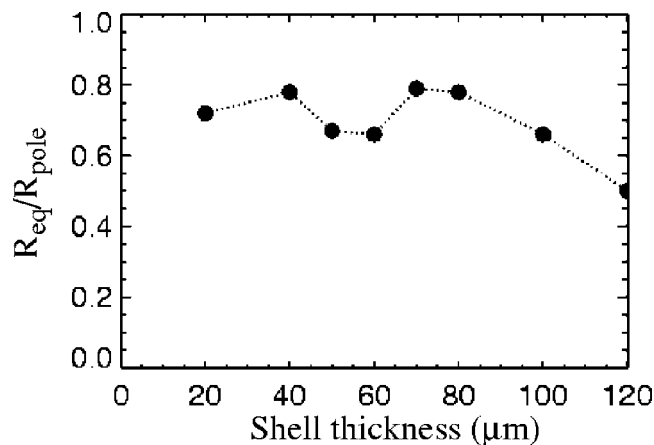


FIG. 22. The ratios of the fuel radius at the equator to the fuel radius at the pole, as calculated by integrated 2D simulations at the times of peak electron temperature, are plotted as a function of the capsule shell thickness. The capsules had a diameter of 2 mm.

sule diameter and shell thickness. Note that the radiation temperature driving the capsule should be nearly unaffected by the capsule diameter and wall thickness as long as the capsule implodes before the shock interacts with the ablation plasma from the capsule, as is the case for all the capsules we are presently considering. However, the radiation asymmetry at the capsule will depend on the case-to-capsule ratio and thus be larger for larger diameter capsules.

The asymmetry of the capsule implosions can be parameterized by the ratio of the CH/deuterium interface at the equator and the pole at peak mass-averaged deuterium electron temperature. This ratio is plotted for 2 mm diameter capsules as a function of the CH shell thickness in Fig. 22. The results indicate that this ratio does not vary much (0.7–0.8) over the thickness range 40–80 μm that has been tested experimentally. The ratio starts to fall significantly for shell thicknesses greater than 80 μm . A much stronger behavior would be expected if the capsule diameters were decreased so that the capsules were ablatively driven, but as we have mentioned this would preclude spectroscopically diagnosing the core using argon x-ray lines. This is because ablatively driven capsules have a much larger areal density of the shell material than exploding pusher capsules at the time of peak core temperature. It may seem counterintuitive that decreasing the diameter of the capsule, while maintaining the shell thickness, would result in an increase in the areal density of the shell material at implosion time. However, it must be remembered that capsules implode sooner as the diameter is reduced and thus experience lower peak radiation temperatures, since the radiation temperature monotonically increases in a dynamic hohlraum. Thus the implosion remains ablative longer for smaller diameter capsules, which results in larger areal densities of the shell.

The asymmetry of the imploded core can be used to infer the average asymmetry of the radiation drive.¹⁷ To interpret our 2D integrated simulations in terms of an average radiation asymmetry we have performed a series of 2D LASNEX simulations of capsule implosion with a time-independent asymmetry characterized by the amplitude of the second

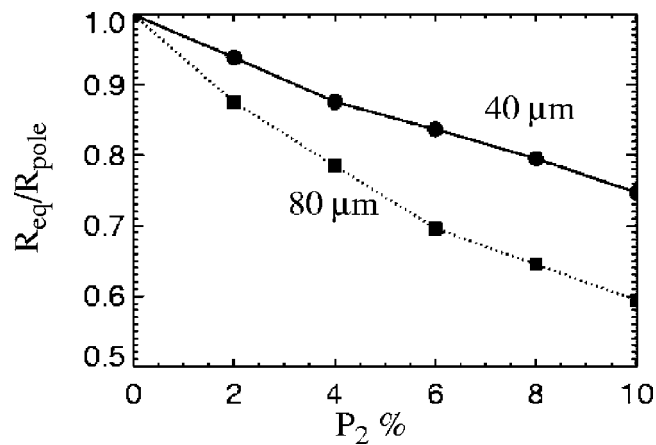


FIG. 23. The ratios of the fuel radius at the equator to the fuel radius at the pole at the time of peak electron temperatures are plotted as a function of the magnitude of the second Legendre mode, P_2 . These results were obtained from 2D simulations of capsules driven with a time dependent radiation drive taken from the integrated simulations, but with a time independent asymmetry P_2 .

Legendre mode P_2 . The time dependence of the radiation temperature driving these capsule simulations, was determined from an unperturbed 2D integrated simulation. The results are shown in Fig. 23, which is a plot of the core asymmetry at peak mass averaged deuterium temperature as a function of P_2 , for 2 mm diameter CH shell capsules of two different wall thicknesses. Comparing Figs. 22 and 23 indicates that the average radiation asymmetry in the 2D integrated simulations is in the range of $P_2=4\%–10\%$. The experimental techniques to accurately measure the ratio $R_{\text{eq}}/R_{\text{pole}}$ are under development.

Presently we have data from a number of experiments using CH capsules, but there was considerable variation in this ratio from shot to shot. This is probably due to the rough surface finish caused by the PVA (polyvinyl-alcohol) coating that is needed to keep these capsules from leaking. The development of much smoother beryllium capsules should allow this measurement to be made with more confidence. Preliminary results with beryllium capsules suggest that the radiation field within the dynamic hohlraum may be more symmetric than predicted by the simulations. Details of these experiments will be presented in a future paper.

VI. CONCLUSIONS AND FUTURE WORK

We have presented 2D integrated simulations of capsule implosions driven by the radiation field generated within dynamic hohlraums. These simulations predicted a number of features that are in good agreement with experimentally measured quantities. The simulations predicted an increase in yield with capsule diameter (2–3 mm) and shell thickness (40–80 μm). The dependence of the yield on capsule diameter was observed early in the experimental program, but the early experiments did not show an increased yield with shell thickness. Later this trend was also observed in the data. We believe that this is due to improved capsule fabrication that resulted in smoother shell surfaces, even though the simulations indicated that the capsules act essentially as exploding

pushers due to the relatively thin walls. We have performed high resolution 2D capsule simulations and found that the yield depends on surface roughness due to the ablative/compressive phase of the shell implosion. Indeed, the predicted neutron yields are within a factor of 2 of the measured yields for capsules with smooth surfaces such as glass and beryllium. This is remarkably good agreement considering the complex nature of the dynamic hohlraum implosion using wire arrays.

Despite these good agreements, there are some significant differences between the predictions of the simulations and some experimentally measured quantities. Spectroscopic measurements of the core conditions indicate that the peak average deuterium density is about a factor of 2 higher than predicted by the simulations, while the average deuterium temperature is about 70% of the simulation results. Capsule simulations indicate that this discrepancy is probably caused by a more slowly rising radiation temperature driving the capsule than predicted by the unperturbed 2D simulations. It was also found that the shock wave velocity predicted by the simulations is significantly higher (40–45 cm/ μ s) than measured in the experiments (\sim 33 cm/ μ s). The slower shock velocity would almost certainly result in a slower rising radiation temperature within the hohlraum. We suspect that the reduced velocity could be due to instability generated turbulence within the wire-array plasma. We have performed 2D simulations with density perturbations in the wire array, which did not reduce the shock velocity or fully develop turbulence. This is probably due to inadequate grid resolution and the reduced dimensionality of these simulations, since turbulence is intrinsically a 3D phenomenon. However, the resulting bubble and spike structure caused the high-z wire-array plasma to be less effective at trapping radiation within the hohlraum. This increased the risetime of the radiation temperature profile driving the capsule, which increased the peak mass averaged deuterium density and reduced the peak mass averaged deuterium electron temperature. Density perturbations of sufficient amplitude to significantly affect the capsule core conditions also cause very thin regions within the simulated wire-array plasma at the time of high radiation temperature. Since the wire-array plasma is acting as the hohlraum case, this could result in radiation drive asymmetries that are random in nature. Measurements are presently underway to determine if there are regions of small optical depth within the wire-array plasma. If so, the dynamic hohlraum will have to be redesigned to mitigate this problem. One approach would be to add high-z material to the outside of the convertor.¹⁶

It may be that turbulence generates a turbulent pressure which decreases the average density within the wire-array plasma. This would reduce the ram pressure that drives the shock within the convertor. Fully resolved 3D simulations would probably shed light on this process, but would require very large computer resources. We plan to pursue an alternate subgrid approach based on a K-epsilon model of turbulence.²⁹

The ability to perform fully integrated simulations is critical for studying the effect of radiation asymmetries on the capsule implosions. Our simulations predict that the core

implosions should be asymmetric with a ratio of the equatorial/polar radii of about 0.7–0.8 at the time of peak fuel temperature. This is consistent with the results of experiments using CH capsules, but there was considerable variation in this ratio from shot to shot, possibly due to the rough capsule surface finish or due to instabilities in the wire-array plasma. The development of much smoother beryllium capsules should allow this measurement to be made with more confidence.

ACKNOWLEDGMENTS

We wish to thank George Zimmerman, Judy Harte, and Lee Busby for LASNEX support and Marty Marinak for help with the HYDRA code. We also thank D. Steinman and the General Atomics fabrication team. We gratefully acknowledge the support of Diana Schroen and the Z crew.

This work was performed at Sandia National Laboratories. Sandia is a multiprogram laboratory operated by Sandia Corporation, a Lockheed Martin company, for the United States Department of Energy under Contract No. DE-AC04-94AL85000.

¹R. B. Spielman, C. Deeney, G. A. Chandler, M. R. Douglas, D. L. Fehl, M. K. Matzen, D. H. McDaniel, T. J. Nash, J. L. Porter, T. W. L. Sanford *et al.*, *Phys. Plasmas* **5**, 2105 (1998).

²V. P. Smirnov, *Plasma Phys. Controlled Fusion* **33**, 1697 (1991).

³J. H. Brownell and R. L. Bowers, *Bull. Am. Phys. Soc.* **40**, 1848 (1995); J. H. Brownell, R. L. Bowers, K. D. McLenithan, and D. L. Peterson, *Phys. Plasmas* **5**, 2071 (1998).

⁴D. D. Ryutov, M. S. Derzon, and M. K. Matzen, *Rev. Mod. Phys.* **72**, 167 (2000).

⁵T. W. L. Sanford, R. B. Spielman, G. O. Allshouse *et al.*, *IEEE Trans. Plasma Sci.* **26**, 1086 (1998).

⁶D. L. Peterson, R. L. Bowers, W. Matuska, K. D. McLenithan, G. A. Chandler, C. Deeney, M. S. Derzon, M. Douglas, M. K. Matzen, T. J. Nash, and N. F. Roderick, *Phys. Plasmas* **6**, 2178 (1999).

⁷T. J. Nash, M. S. Derzon, G. A. Chandler, R. Leeper, D. Fehl, J. Lash, C. Ruiz, G. Cooper, J. F. Seaman, J. McGurn *et al.*, *Phys. Plasmas* **6**, 2023 (1999).

⁸C. Deeney, M. R. Douglas, R. B. Spielman, T. J. Nash, D. L. Peterson, P. L'Epattenier, G. A. Chandler, J. F. Seaman, and K. W. Struve, *Phys. Rev. Lett.* **81**, 4883 (1998).

⁹S. A. Slutz, R. A. Vesey, J. E. Bailey, G. A. Chandler, and W. S. Varnum, *Bull. Am. Phys. Soc.* **46**, 106 (2001).

¹⁰S. A. Slutz, J. E. Bailey, G. A. Chandler, G. R. Bennett, G. Cooper, J. S. Lash, S. Lazier, P. Lake, R. W. Lemke, T. A. Mehlhorn *et al.*, *Phys. Plasmas* **10**, 1875 (2003).

¹¹C. L. Ruiz, G. W. Cooper, S. A. Slutz, J. E. Bailey, G. A. Chandler, T. J. Nash, T. A. Mehlhorn, R. J. Leeper, D. Fehl, A. J. Nelson, J. Franklin, and L. Ziegler, *Phys. Rev. Lett.* **93**, 015001 (2004).

¹²S. A. Slutz, M. R. Douglas, J. S. Lash, R. A. Vesey, G. A. Chandler, T. J. Nash, and M. S. Derzon, *Phys. Plasmas* **8**, 1673 (2001).

¹³J. Lash, G. A. Chandler, G. Cooper, M. S. Derzon, M. R. Douglas, D. Hebron, R. J. Leeper, M. K. Matzen, T. A. Mehlhorn, T. J. Nash, R. E. Olson, C. L. Ruiz, T. W. L. Sanford, S. A. Slutz, D. L. Peterson, and R. E. Chrien, "The prospects for high yield ICF with a Z-pinch driven dynamic hohlraum," in *Proceedings of Inertial Fusion Science and Applications 99, Bordeaux, FR, September 1999*, edited by C. Labaune, W. J. Hogan, and K. A. Tanaka (Elsevier, Paris, 2000), Vol. I, p. 583.

¹⁴J. D. Lindl, P. Amendt, L. Berger, S. G. Glendinning, S. H. Glenzer *et al.*, *Phys. Plasmas* **11**, 339 (2004).

¹⁵R. W. Lemke, J. E. Bailey, G. A. Chandler, T. J. Nash, S. A. Slutz, and T. A. Mehlhorn, *Phys. Plasmas* **12**, 012703 (2005).

¹⁶S. A. Slutz, R. A. Vesey, D. L. Hanson, R. B. Campbell, T. A. Mehlhorn, M. E. Cuneo, and J. L. Porter, *Plasma Phys. Controlled Fusion* **47**, B851 (2005).

¹⁷A. A. Hauer, L. Suter, N. Delamater, N. Delamater, D. Ress, L. Powers,

- G. Magelssen, D. Harris, O. Landen, E. Lindmann *et al.*, Phys. Plasmas **2**, 2488 (1995).
- ¹⁸G. B. Zimmerman and W. L. Kruer, Comments Plasma Phys. Controlled Fusion **2**, 51 (1975).
- ¹⁹J. P. Chittenden, S. V. Lebedev, S. N. Bland, A. Ciardi, and M. G. Haines, Phys. Plasmas **8**, 675 (2001).
- ²⁰S. V. Lebedev, F. N. Beg, S. N. Bland, J. P. Chittenden, A. E. Dangor *et al.*, Phys. Plasmas **8**, 3734 (2001).
- ²¹N. F. Roderick, T. W. Hussey, R. J. Faehl, and R. W. Boyd, Appl. Phys. Lett. **32**, 273 (1978).
- ²²J. E. Bailey, G. A. Chandler, G. A. Rochau, Y. Maron, S. A. Slutz, G. S. Dunham, I. Golovkin, P. W. Lake, R. W. Lemke, J. M. Lucas *et al.*, High energy density physics **1**, 21 (2005).
- ²³J. E. Bailey, G. A. Chandler, S. A. Slutz, G. R. Bennett, G. Cooper, J. S. Lash, S. Lazier, R. Lemke, T. J. Nash, D. S. Nielsen, T. C. Moore, C. L. Ruiz, D. G. Schroen, R. Smelser, J. Torres, and R. A. Vesey, Phys. Rev. Lett. **89**, 095004 (2002).
- ²⁴M. M. Marinak, G. D. Kerbel, N. A. Gentile, O. Jones, D. Munro, S. Pollaine, T. R. Dittrich, and S. W. Hahn, Phys. Plasmas **8**, 2275 (2001).
- ²⁵M. D. Rosen and J. H. Nuckols, Phys. Fluids **22**, 1393 (1979).
- ²⁶J. E. Bailey, G. A. Chandler, R. C. Mancini, S. A. Slutz, G. A. Rochau, M. Bump, T. J. Burris-Mog, G. Cooper, G. Dunham, I. Golovkin *et al.*, Phys. Plasmas **13**, 056301 (2006).
- ²⁷J. E. Bailey, G. A. Chandler, S. A. Slutz, I. Golovkin, P. W. Lake, J. J. MacFarlane, R. C. Mancini, T. J. Burris-Mog, G. Cooper, R. J. Leeper *et al.*, Phys. Rev. Lett. **92**, 085002 (2004).
- ²⁸R. W. Lemke, J. E. Bailey, G. A. Chandler, T. J. Nash, S. A. Slutz, and T. A. Mehlhorn, Phys. Plasmas **12**, 012703 (2005).
- ²⁹J. H. Hammer and G. B. Zimmerman, Bull. Am. Phys. Soc. **50**, 8 (2005).